ADVANCES IN ATMOSPHERIC SCIENCES, VOL. 21, NO. 5, 2004, 708–716

A Numerical Study of a TOGA-COARE Squall-Line Using a Coupled Mesoscale Atmosphere-Ocean Model

Shaowu BAO*, Lian XIE, and Sethu RAMAN

Department of Marine, Earth and Atmospheric Sciences, North Carolina State University, Box 8208, *Raleigh, NC* 27695-8208

(Received 24 March 2003; revised 8 April 2004)

ABSTRACT

An atmosphere-ocean coupled mesoscale modeling system is developed and used to investigate the interactions between a squall line and the upper ocean observed over the western Pacific warm pool during the Tropical Ocean/Global Atmosphere Coupled Ocean and Atmosphere Response Experiment (TOGA-COARE). The modeling system is developed by coupling the Advanced Regional Prediction System (ARPS) to the Princeton Ocean Model (POM) through precipitation and two-way exchanges of momentum, heat, and moisture across the air-sea interface. The results indicate that the interaction between the squall-line and the upper ocean produced noticeable differences in the sensible and latent heat fluxes, as compared to the uncoupled cases. Precipitation, which is often ignored in air-sea heat flux estimates, played a major role in the coupling between the mesoscale convective system and the ocean. Precipitation affected the air-sea interaction through both freshwater flux and sensible heat flux. The former led to the formation of a thin stable ocean layer underneath and behind the precipitating atmospheric convection. The presence of this stable layer resulted in a more significant convection-induced sea surface temperature (SST) change in and behind the precipitation zone. However, convection-induced SST changes do not seem to play an important role in the intsensification of the existing convective system that resulted in the SST change, as the convection quickly moved away from the region of original SST response.

Key words: air-sea interaction, mesoscale modeling, squall line, coupled ocean-atmosphere modeling

1. Introduction

Air-sea interaction plays an important role in the global seasonal to inter-annual climate variability, most notably, the El Niño and Southern Oscillation (ENSO) phenomenon (Webster and Lukas, 1992). Because of its widespread impacts on global weather and climate, air-sea interaction has been extensively investigated and its importance in seasonal to inter-annual climate prediction is well documented. Recent studies revealed the significance of mesoscale air-sea interactions in coastal atmospheric and oceanic processes (Xie et al., 1999), associated with the development of tropical cyclones (Emanuel, 2001), and in tropical convection (Barnes, 1994). Barnes (1994) stated that the ocean and atmosphere in the Tropics communicate on the meso scale. Mesoscale precipitation systems play an important role in the ENSO cycle. Such precipitation systems are also connected with westerly wind bursts over the equatorial western Pacific, which sometimes trigger the onset of the ENSO events (Richardson et al., 1999).

However, mesoscale air-sea interactions in the Tropics are not well understood due to inefficient observational data over tropical oceans. For example, not much is known about the western Pacific precipitation systems–their structure, how they form, how they impact the upper ocean, and how the upper ocean's feedback effects affect the atmosphere. Although tropical convection and its effect on the ocean have been studied extensively, the effect of precipitation on the air-sea interaction associated with tropical convection has not been addressed adequately. TOGA/COARE (Tropical Ocean-Global Atmosphere/Coupled Ocean-Atmosphere Response Experiment) conducted from 1992 to 1993 over the tropical western Pacific provided a unique opportunity to study the interactions between atmospheric convection and the upper ocean.

*E-mail: sbao@unity.ncsu.edu

Table 1. Experiment design for the simulations of air-sea interaction using the coupled modeling system.

Model	ΔT (s)	ΔX (m) ΔY (m)	Minimum ΔZ(m)	Turbulent Closure Scheme	Lateral BC
ARPS	6	3000	100	TKE Order 1.5	Radiation (open) Lateral boundary
POM	6	3000	1	Mellor Yamada Order 2.5	Radiation(open) Lateral boundary

The region of the western Pacific where sea surface temperature (SST) is higher than 28°C is known as the western Pacific warm pool (WPWP). Because of the high SST, the western Pacific warm pool supplies the atmosphere with large amounts of heat and moisture that result in substantial annual tropical precipitation. There were many squall lines over the WPWP region during the TOGA COARE experiment. In this paper, a well documented squall line on 22 February 1993 was simulated using the ARPS (Advanced Regional Prediction System) model. This squall line has been investigated by Jorgensen (1995), Trier et al. (1996), Hong et al. (1999), and Bao et al. (2003). The study of Bao et al. (2003) showed that precipitation associated with tropical convection, among others factors, appears to play an important role in affecting the dynamics of the upper ocean. Rain water, which is significantly cooler than the sea surface, cools the upper ocean. Rain water causes the density of the ocean's surface layer to decrease, thus forming a thin low salinity, low density stable layer near the surface. This thin layer accelerates the upper ocean's response to the atmosphere.

The principal goal of this study is to improve the understanding of the mesoscale air sea interaction processes in the WPWP. The authors try to answer the following two questions: how does the accelerated oceanic response (Bao et al., 2003) affect the atmospheric processes that produced the precipitation in the first place? What, if any, effect does precipitation have on mesoscale air-sea interaction?

This study extends the work of Bao et al. (2003) and Trier et al. (1996) by using a coupled model. It extends the study of Hong et al. (1999) by including precipitation (see Eq. 5 and Eq. 6). The improvements in the understanding of the mesoscale air-sea interaction mechanisms could lead to better parameterization of air-sea fluxes and ultimately improved coupled climate models for seasonal to inter-annual prediction. A brief description of the coupled modeling system used in this study is presented in section 2. Section 3 lists the experiments carried out in the study. Section 4 presents and discusses the results of the upper ocean's response to a squall line and its feedback effects on the atmosphere. Conclusions are summarized in section 5.

2. Model description

The modeling system is comprised of two interactively coupled models: a mesoscale atmospheric model and a regional ocean circulation model. The configurations of the two models are summarized in Table 1.

The atmospheric component of the coupled modeling system is the ARPS model. The ARPS model has been developed at the Center for Analysis and Prediction of Storms (CAPS) at the University of Oklahoma (Xue et al., 2000). It is a non-hydrostatic atmospheric prediction model and can be used to study atmospheric motions with horizontal scales ranging from a few meters to hundreds of kilometers. The ARPS model is based on compressible Navier-Stokes equations describing the atmospheric flow, and it uses a generalized terrain-following coordinate system. Turbulence parameterization, which is a planetary boundary layer (PBL) closure linking the resolved scale and the unresolved subgrid-scale motions, is critical to the successful simulation of many flows. In this study, a 1.5-order Turbulence Kinetic Energy (TKE) closure is used to compute the turbulent mixing. A six-phase water/ice cloud microphysics scheme based on the Kessler scheme (Kessler, 1996) is used to simulate the cloud processes. A stability and roughness-length dependent surface flux model (Businger et al., 1971) is used to compute the surface fluxes. The surface fluxes enter the model as the lower boundary conditions for the turbulent momentum and sensible and latex heat fluxes.

The center of the simulation domain is located at (9°S, 160°E) because of the availability of observations in this region. A generalized terrain-following coordinate with equal spacing in the x and y directions and grid stretching in the vertical is used. The simulation domain is 540 km×180 km with a horizontal resolution of 3 km. A hyperbolic tangent vertical stretching is used to enhance the vertical resolution of the low-level grids. The initial condition described by a single sounding is assumed to be horizontally homogeneous in the entire simulation domain.

A low-level (at an altitude of 150 m) negative potential temperature anomaly of 8 K is used to initialize the convection. The initial potential temperature

perturbation also has an orientation of 150° to 330°, which is consistent with the shape of the observed convective line.

The Princeton Ocean Model (POM) model is used as the oceanic component of the coupled system. It contains an imbedded second moment turbulence closure model to provide vertical mixing coefficients. It also uses a terrain following (σ) coordinate in the vertical, where $\sigma = (Z-\eta)/(H+\eta)$. Z is the conventional Cartesian vertical coordinate. $D \equiv H + \eta$, where H is the mean bottom depth and η is the surface elevation. The horizontal time differencing is explicit whereas the vertical differencing is implicit. The latter eliminates time constraints for the vertical coordinate and permits the use of fine vertical resolution in the surface and bottom boundary layers. The model has a free surface and uses a split time step. The external mode portion of the model is two-dimensional and uses a short time step based on the Courant-Friedrich-Levy (CFL) condition and the external wave speed. The internal mode is three-dimensional and uses a larger time step based on the CFL condition and the internal wave speed. Complete thermodynamics have been implemented. Details of the model are described by Blumberg and Mellor (1987) and Kantha and Clayson (2000).

The horizontal resolution of the ocean model is also set to 3 km, which is the same as that in the atmospheric component. A stretching vertical grid scheme is used. A higher vertical resolution is used for the upper layers because the ocean's response to the surface atmospheric forcing such as precipitation associated with squall lines, which lasts for only a few hours, occurs mainly in the upper ocean. Below a depth of 50 m, the ocean's response is not significant. In this study, the finest vertical resolution, at the upper-most layer, is about one meter. The ocean model uses a time-split technique to improve model efficiency. A smaller time step (6 s) is used for the faster external mode, and a much larger time step (180 s) is used for the slower internal mode. The ocean model is initialized with climatic temperature and salinity profiles based on the Levitus data (Levitus and Boyer, 1994; Levitus et al., 1994).

The parameterization of the turbulent mixing processes is critical in the simulation of the upper ocean boundary layer response to the atmospheric forcing. The second moment turbulent closure model included in POM, often cited in the literature as the Mellor-Yamada turbulent closure model (Mellor and Yamada, 1982), is widely used in geophysical fluid studies because it is relatively simple and still retains much of the second moment accuracy.

Air-sea coupled numerical models that include the material and energy transfer processes (momentum, salinity, and sensible and latent heat fluxes) are useful tools for mesoscale air-sea interaction studies. Direct observations of mesoscale air-sea interactions are difficult and usually limited to a few specialized platforms, and thus are often insufficient to properly describe mesoscale convection processes such as the ones occurring in a squall line whose time scales are only a few hours. On the other hand, space-based observations of the sea surface conditions are often contaminated by the presence of deep clouds covering the sea surface during deep convective processes. Thus coupled numerical models are not only useful, but also often a necessity.

Because the exchange processes across the air-sea interface cannot be quantified analytically, parameterization of the air-sea fluxes is generally used in mesoscale and climate models. In this study, the bulk aerodynamic method (Eqs. (1)–(4)), a commonly used parameterization model, is used to estimate the momentum, heat, and moisture fluxes across the air-sea interface.

$$\overline{(u'w')}_s = -C_{\mathrm{D}}\overline{M}\overline{U} \,, \tag{1}$$

$$\overline{(v'w')}_s = -C_{\mathrm{D}}\overline{M}\overline{V} \,, \tag{2}$$

$$\overline{(q'w')}_s = -C_{\mathrm{E}}\overline{M}\,(\overline{q} - q_{\mathrm{G}}) \,, \tag{3}$$

$$\overline{(\theta'w')}_s = -C_{\mathrm{H}}\overline{M}\,(\overline{\theta} - \theta_{\mathrm{G}}) \,, \tag{4}$$

where $\overline{(u'w')}_s$ and $\overline{(v'w')}_s$ are momentum fluxes, $\overline{(q'w')}_s$ is moisture flux, $\overline{(\theta'w')}_s$ is heat flux, C_{D} is drag coefficient, C_{H} and C_{E} are bulk transfer coefficients for heat and moisture, respectively, $\overline{M}$ is mean horizontal wind magnitude above the surface, $\overline{U}$ and $\overline{V}$ are mean horizontal wind vectors above the surface, $\overline{\theta}$ and $\overline{q}$ are mean potential temperature and moisture above the sea surface, θ_{G} and q_{G} are mean potential temperature and moisture at the surface.

The calculated $\overline{(u'w')}_s$, $\overline{(v'w')}_s$, $\overline{(q'w')}_s$, and $\overline{(\theta'w')}_s$ are used as the bottom boundary conditions for the atmosphere model and as the top boundary conditions in the ocean model.

The rain water–cooler than ocean's surface water–enters the sea water and has the effect of reducing the upper ocean's salinity and temperature. The rainfall-induced freshwater flux (F_s) and heat flux (F_t) are given by Curry and Webster (1999):

$$F_s = \rho I S_0 \,, \tag{5}$$

$$F_t = \rho c_p I (T_{\mathrm{a}} - T_0) \,, \tag{6}$$

where ρ is water density, I is rainfall intensity, S_0 is surface salinity, c_p is specific heat of liquid water (4218 J K^{-1} kg^{-1}), T_{a} is atmospheric temperature near the

surface and assumed to be equal to rain drop temperature, T_0 is sea surface temperature.

The upper ocean's salinity and temperature variations caused by precipitation-induced freshwater flux

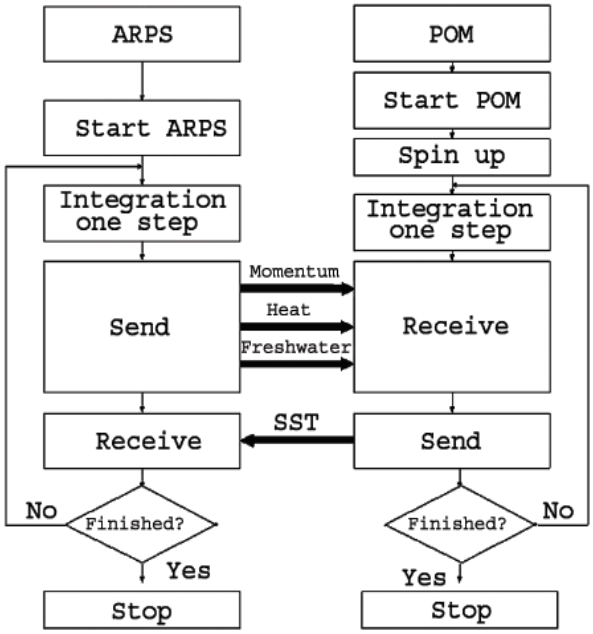

Fig. 1. Schematic illustration of the method used in coupling the ARPS and POM models.

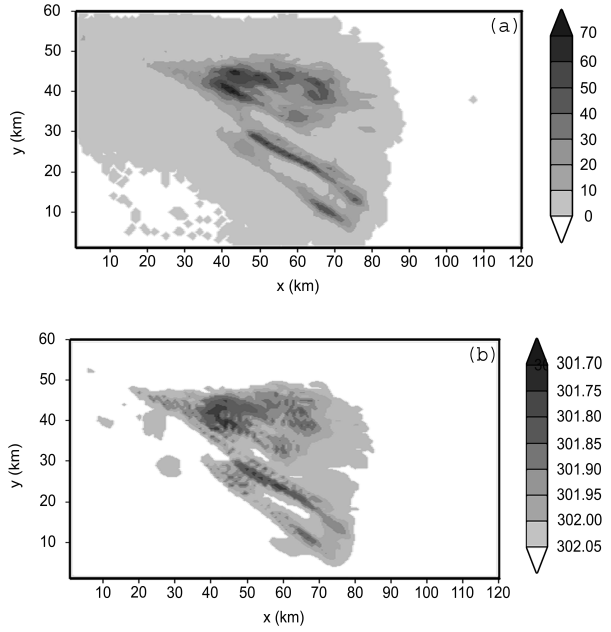

Fig. 2. Simulated evolution of the (a) accumulated rainfall amount (in mm) and (b) corresponding sea surface temperature (SST) variations (in K) at 5 h of integration time in EXPT. 1.

agree and observation averaged from 6 June to 7 July 2001.well with observations (Wijesekera et al., 1999).

A Message Passing Interface (MPI) is used to communicate between the ARPS and POM models. MPI, used widely on almost all multi-processor computing platforms, is a library that provides a powerful, efficient, and portable way to implement parallel computation. Using MPI, two separate programs can exchange data concurrently. In this case, the ARPS model and POM model can exchange momentum, heat, and freshwater fluxes and sea surface temperature at every time step. The data communication procedure is illustrated in Fig. 1.

3. Experiment design

In this study, five experiments are conducted to investigate whether the SST variation due to the precipitation has any effect on the atmosphere and, in particular, the convection processes (Table 2). A squall line observed during TOGA COARE TOGA-COARE is used as the test case. This case is chosen because it has been extensively investigated in the past by Jorgensen et al. (1995), Trier et al. (1996) and Hong et al. (1999), so comparisons with the results from existing studies can be easily made. In EXPT. 1, both the oceanic responses to the squall line and the SST's feedback effects on the atmosphere are investigated. That is, in the ARPS model, the bottom boundary condition is updated to include the SST variation simulated in POM. In a companion experiment, EXPT. 2, all the model configurations are the same as in EXPT. 1 except that the SST variation in the POM model is not communicated to the atmosphere. The difference between the simulated results in EXPT. 1 and EXPT. 2 are analyzed to investigate the SST's feedback effects on the atmosphere. EXPT. 3, EXPT. 4 and EXPT. 5 are conducted to investigate the different roles of the sensible heat flux, latent heat flux, rainfall-induced heat flux, and rainfall-induced salinity flux in affecting the SST. The experiments are listed in Table 2.

4. Results and discussion

4.1 *Oceanic response to squall line*

The simulated evolution of SST variations and the corresponding accumulated rainfall amounts for EXPT. 1 are shown in Fig. 2. It is apparent that with an increase in the accumulated rainfall amount, the SST in the rainfall covered region decreases. At $t = 5$ h, the maximum accumulated rainfall amount reached

Table 2. List of sensitivity experiments.

	EXPT. 1	EXPT. 2	EXPT. 3	EXPT. 4	EXPT. 5
Ocean's feedback effects	Included	Not included	Included	Included	Included
Rainfall-induced heat flux	Included	Included	Included	Not included	Not included
Rainfall induced freshwater flux	Included	Included	Included	Not included	Included
Sensible and latent heat fluxes	Included	Included	Not included	Included	Included

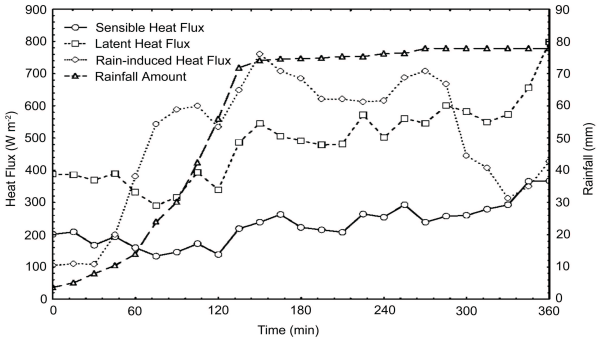

Fig. 3. Time series of the simulated maximum rainfall amount (in mm), sensible, latent, and rainfall-induced heat fluxes (in W m^{-2}) across the air-sea interface during the life cycle of the simulated squall line.

70 mm and the maximum SST anomaly reached 0.35°C. In addition, the pattern of the SST anomaly resembles that of the accumulated rainfall, and the maximum SST anomaly is in the same location as the maximum accumulated rainfall.

It should be pointed out, however, that although precipitation plays an important role in affecting the SST, the effect of sensible and latent heat fluxes cannot be neglected. Actually even during the squall line processes, which lasted for only a few hours, the magnitudes of the sensible and latent heat fluxes were comparable to that of raindrop-induced sensible heat flux. The time series of the maximum heat transferred across the air-sea interface by the sensible (Eq. (4)), latent (Eq. (3)), and rainfall-induced (Eq. (6)) heat fluxes during the simulated squall line process are shown in Fig. 3. It is clear that at the beginning of the simulation, the rainfall amount is small, whereas the sensible and latent heat fluxes are greater than the rainfall-induced heat flux. With the increase of rainfall amount, the rainfall-induced heat flux increases rapidly and surpasses the sensible and latent heat fluxes. The accumulated rainfall amount increases until $t = 140$ min. With no further rainfall, the maximum rainfall-induced heat flux levels off and subsequently begins to decrease. During the rainfall process, the rainfall-induced heat flux is larger than the sensible and latent heat fluxes.

Note that the sensible, latent, and rainfall-induced heat fluxes have comparable magnitudes, but the SST variation appears to be mainly determined by the accumulated rainfall. To understand why this is the case, we carried out several sensitivity experiments (Table 2) in which the salinity variation is not included. EXPT. 3, EXPT. 4, and EXPT. 5 are conducted to investigate the different roles of the sensible

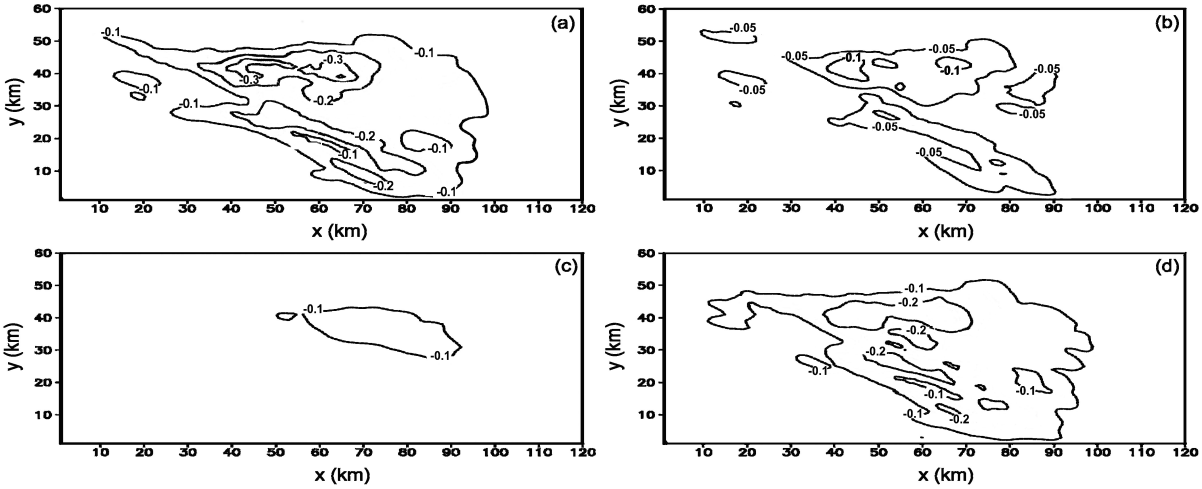

Fig. 4. Simulated SST variations (in K) in (a) EXPT. 1 (b) EXPT. 3 (c) EXPT. 4 (d) EXPT. 5 at 6 h of integration time. Notice that the SST variation is sensitive to the inclusion of rainfall-induced freshwater flux.

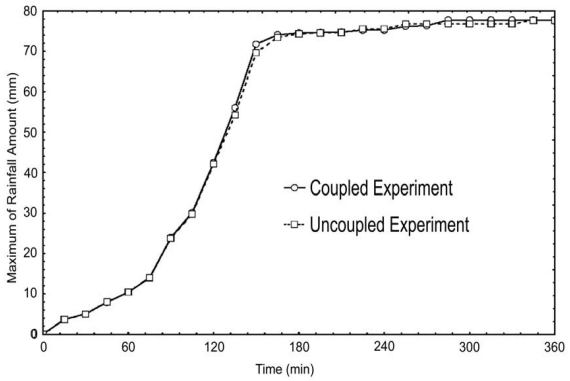

Fig. 5. Time series of the simulated maximum of accumulated rainfall amount (in mm) in the coupled and uncoupled experiments. There is no significant difference in the simulated rainfall amount between the two.

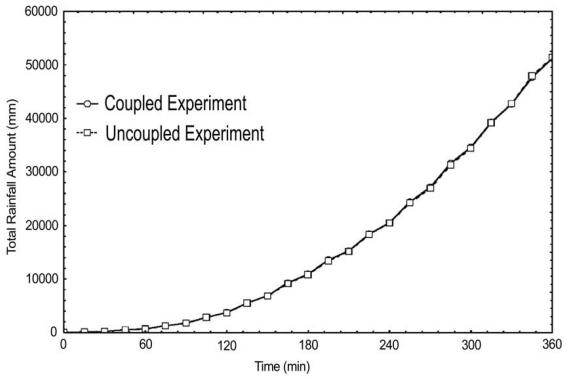

Fig. 6. Time series of the simulated total accumulated rainfall amount (in mm) in the coupled and uncoupled experiments. Notice there is no significant difference in the simulated rainfall amount between the two.

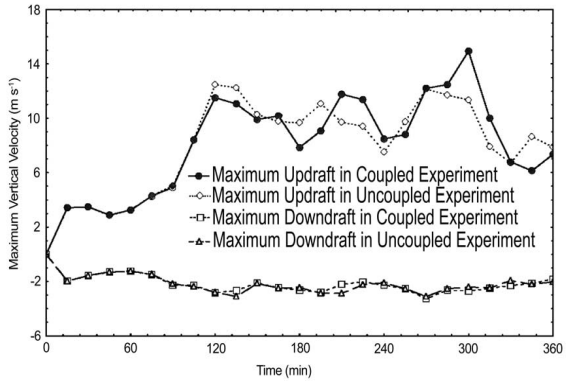

Fig. 7. Time series of simulated maximums of updrafts and downdrafts (in m s^{-1}) in the coupled and uncoupled experiments. There is no significant difference in the simulated updrafts and downdrafts between the coupled and uncoupled experiments.

heat flux, latent heat flux, rainfall-induced heat flux, and rainfall-induced freshwater flux in affecting the SST in the coupled model.

Figure 4 shows the simulated SST variations in (a) EXPT. 1 (b) EXPT. 3 (c) EXPT. 4, and (d) EXPT. 5. It is clear from Fig. 4 that when rainfall-induced freshwater flux is included (EXPT. 1, EXPT. 3, and EXPT. 5), the SST variations are significant, no matter whether the rainfall-induced heat flux or the sensible and latent heat fluxes are included. EXPT. 4 has the same configuration as EXPT. 5 except that in EXPT. 5, the rainfall-induced freshwater flux is included while in EXPT. 4 it is not. When the rainfall-induced freshwater flux is not included, as in EXPT. 4, the SST variation is not significant. These results suggest that the rainfall-induced stable fresh water layer is a key factor in determining the SST change.

Raindrops enter the upper ocean as cool freshwater flux and cause a thin low temperature, low salinity and low density stable layer. This thin stable layer isolates the surface layer from the rest of the upper ocean and blocks the turbulent exchange of mass and energy between the sea surface and below. Therefore, in the rainfall-covered region, the cooling effects are accumulated near the surface and the SST variations are significant and last longer. In the regions not covered by rainfall, the heat fluxes, although of similar magnitude as those in the rainfall-covered region, are transferred downward quickly from the ocean's surface to the mixed layer by turbulent mixing.

4.2 *The effects of SST variation on atmospheric convection*

The simulation results described above showed that the tropical convection can have significant effects on the upper ocean. However, one important question that remains unanswered is whether the rainfall-induced SST variation can, in turn, influence the atmospheric processes.

EXPT. 1 and EXPT. 2 were carried out to investigate the coupling effects. Some important features of the simulated squall line process, including the rainfall amount, maximum updraft and downdraft, and cloud top heights were compared between the coupled (EXPT. 1) and uncoupled (EXPT. 2) experiments.

The time series of the simulated maximum accumulated rainfall amount in the coupled and the uncoupled experiments is shown in Fig. 5. The time series of the simulated total accumulated rainfall amounts for the coupled and the uncoupled experiments are shown in Fig. 6. Comparing Fig. 5 with Fig. 6, it is clear that the rainfall amounts in the coupled and the uncoupled experiments have no significant difference. The maximum updrafts and downdrafts in the coupled and the uncoupled experiments (Fig. 7) show no systematic difference either. The vertical $(X - Z)$ cross sections of the amount of cloud water, cloud ice, and cloud snow

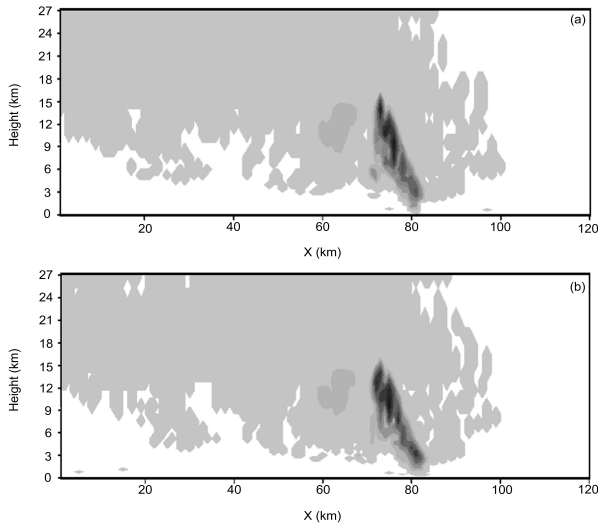

Fig. 8. Vertical ($X - Z$) cross sections of the amount of liquid cloud, ice cloud, and snow cloud made across the locations of the maximum updrafts in the (a) coupled and (b) uncoupled experiments at 4 h of integration time. Notice that no significant difference in cloud height is seen.

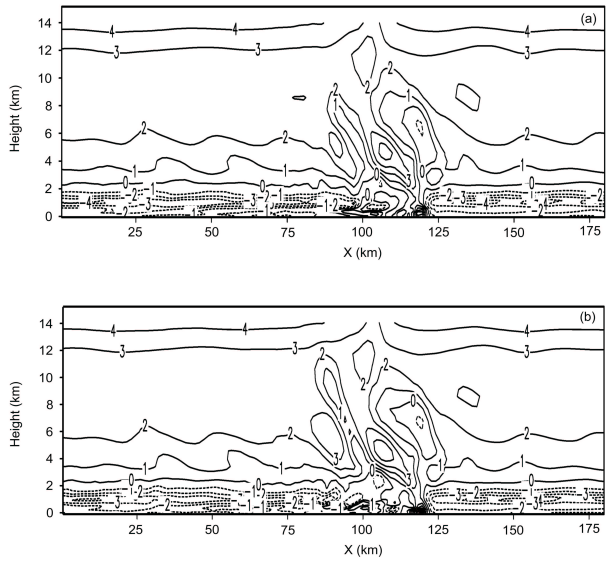

Fig. 9. Vertical cross sections of the vertical gradients of the equivalent potential temperature (K) in the (a) coupled experiments and (b) uncoupled experiments 5 h from the beginning of the simulations. Notice that there is no significant difference apparent between the coupled and uncoupled experiments.

across the locations of the maximum updrafts in the (a) coupled and (b) uncoupled experiments are shown in Fig. 8. The cloud tops reached an altitude of 15000 m at $t = 2$ h (from the beginning of the simulations) and remained at that height for six hours in both the coupled and uncoupled experiments.

The vertical cross sections of the vertical gradients of the equivalent potential temperature are shown in Fig. 9. Equivalent potential temperature, θ_e, shows the temperature that the air would have if it ascended until all the water vapor were condensed out and the air were brought back down to 1000 hPa adiabatically. The negative anomalies in Fig. 9, which indicate decreasing θ_e with height, show the region with potential instability, and the positive anomalies correspond to stable downdraft regions behind the leading edge of the convective lines. It is apparent that no significant difference is seen in Fig. 9 between the simulated potential instabilities in the coupled and the uncoupled experiments. Therefore, the SST's feedback effect does not appear to have a significant effect on the stability profiles of the convective systems in the atmosphere.

The reason that the rainfall-induced SST variation has no significant effect on the convection may be that the tropical squall line process simulated in this study moves in a direction perpendicular to the low level wind shear at a speed of about 12 m s^{-1} (Trier et al., 1996). The SST variations occur over the rainfall covered region, behind the leading edge of the squall line convection. Therefore, in the region where the SST variations are significant, the downdrafts are dominant and the convection is at the stage of dissipation. When the sea surface cooling effects are communicated back to the atmosphere in the rainfall covered region, the active convection has already moved along the direction perpendicular to the low level wind shear to the region where the underlying SST has not been modified by the rainfall. Since the rainfall-induced SST variation is lagging far behind the leading edges of the squall lines, it has no significant effect on the atmosphere convection that produced the rain.

4.3 *The effects of SST variation on air-sea heat fluxes*

Although the simulated SST variation has no significant effect on the atmospheric convection processes, the results show that it does have a significant influence on the sensible and latent heat exchanges across the air-sea interface.

In this study, the only parameter in the ocean model that feeds the atmosphere model is the SST. The spatial pattern of the SST variation corresponds well to the distribution of rainfall. The time series of the total sensible heat flux and latent heat flux across the air-sea surface over the rainfall covered regions in the coupled and the uncoupled experiments are shown in Fig. 10. It is apparent that at the beginning of the simulation, when the rainfall amount is still small, the magnitudes of the sensible and latent heat fluxes over

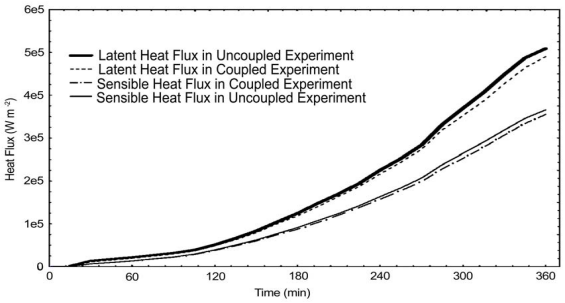

Fig. 10. Time series of the total sensible heat flux and latent heat flux (in W m^{-2}) across the air-sea surface over the rainfall covered regions in the coupled and uncoupled experiments. The simulated sensible and latent heat fluxes differ between the coupled and uncoupled experiments.

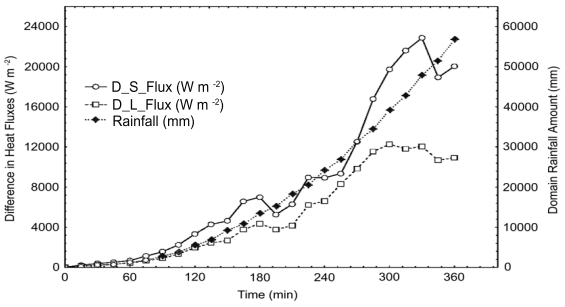

Fig. 11. The time series of the sum of the simulated differences in $\overline{(\theta' w')}_s$ (D_S_FLUX in W m^{-2}), $\overline{(q' w')}_s$ (D_L_FLUX in W m^{-2}), and the rainfall amount (mm) over the rain covered region between the coupled and uncoupled experiments. The variations of the heat fluxes and the rainfall amount have similar patterns indicating their strong correlation.

the rainfall-covered regions are small and no significant difference is seen between the coupled and uncoupled experiments. With the increase in rainfall amount and its coverage, the differences in the heat fluxes between coupled and uncoupled models increase. The difference in the total heat fluxes over the rainfall-covered region between the coupled and uncoupled simulations can be as high as 6% of the simulated value in the coupled experiment. The time-averaged differences in the heat fluxes between the coupled and uncoupled experiments are 3.8% for latent heat flux and 3.2% for sensible heat flux. That means when precipitation is present and if the rainfall-induced heat flux and freshwater flux are neglected, the heat transferred across the air-sea interface will be over-estimated by about 3% to 6%.

In order to validate the argument that the heat flux differences shown in Fig. 10 are the result of the SST variation, a correlation analysis was performed on the differences in the sensible heat flux, latent heat flux, SST, surface moisture, bulk transfer coefficients of heat and moisture, surface velocity and rainfall amount between the coupled and uncoupled experiments. The results are shown in Table 3. In Eq. (3) and Eq. (4), $\theta_{\rm G}, \underline{q_{\rm G}}, \overline{M}, C_{\rm E}$, and $C_{\rm H}$ can affect the sensible heat flux $\overline{(\theta' w')}_s$ and latent heat flux (moisture flux $\overline{(q' w')}_s$). The time series of the simulated rainfall amount and the differences in $\overline{(\theta' w')}_s$ and $\overline{(q' w')}_s$ between the coupled and uncoupled experiments are shown in Fig. 11.

In Table 3 and Fig. 11, the abbreviations are defined as: D_ S_ Flux = Sensible heat flux_uncoupled-Sensible heat flux_ coupled, D_ L_ Flux = Latent heat flux_ uncoupled-Latent heat flux_ coupled, D_ SST = SST_ uncoupled - SST_ coupled, D_ QVS = Sea surface moisture_ uncoupled-Sea surface moisture_ coupled, D_ $C_{\rm H}$=bulk heat transfer coefficient_ uncoupled - bulk heat transfer coefficient_ coupled, D_ $C_{\rm E}$=bulk moisture transfer coefficient_ uncoupled - bulk moisture transfer coefficient_ coupled, D_ M = surface velocity_ uncoupled-surface velocity_ coupled,

From Fig. 11 and Table 3, it is clear that the differences in the sensible and latent heat fluxes have a strong correlation (>0.97) with the SST anomalies and the rainfall.

5. Conclusion

An air-sea coupled numerical modeling system was developed based on the ARPS and the POM. Results from the numerical experiments using this coupled model show that during mesoscale convection processes, sensible, latent, and rainfall-induced heat fluxes have comparable magnitudes. SST variation, however, is determined mainly by the accumulated rainfall amount. The reason that rainfall played a more important role than the sensible and latent heat fluxes in modifying the SST is that the rainfall induces not only heat flux but also salinity flux, which tends to isolate the upper ocean by making it more stable. The isolated upper ocean tends to react much faster to the atmospheric forcing for the case without the rainfall-induced salinity flux.

Although rainfall has significant effects on the SST, the feedback of the SST variation to the atmosphere does not appear to have a significant influence on the existing atmospheric convection. The reason that the SST variation did not affect the existing atmospheric convection process is that the squall line system simulated in this study moved at a speed of about 12 m s^{-1} (Trier et al., 1996). However, numerical results show

Table 3. Correlation of the differences in $\overline{(\theta' w')_s}$, $\overline{(q' w')_s}$, $\theta_G, q_G, C_H, C_E, \overline{M}$, and rainfall amount between the coupled and uncoupled experiments.

	D_S_Flux	D_L_Flux	D_SST	D_QVS	D_C_H	D_C_E	D_M	Rainfall
D S Flux	1.00	0.98	0.97	0.97	0.63	0.63	0.04	0.97
D L Flux	0.98	1.00	0.96	0.96	0.49	0.49	0.22	0.97

that the SST feedback has a significant effect on the air-sea sensible and latent heat fluxes. The difference in the simulated heat fluxes is of the order of 6% when rainfall is included. Therefore, although the SST variation did not have a significant direct effect on the existing convection in the simulation, it changed the atmospheric and oceanic environmental conditions which, to some extent, may have become more favorable for subsequent convective systems to develop. Thus, precipitation-induced air-sea heat and buoyancy fluxes must be properly incorporated in the overall estimates of air-sea fluxes.

Acknowledgments. This work was jointly supported by the Division of Atmospheric Sciences, National Science Foundation under Grant Nos. ATM-9632390 and ATM-0080088, and the National Oceanic and Atmospheric Administration under Grant No. NA03-NES-4400015. The model developments and simulations were performed in the Coastal Fluid Dynamic Laboratory, North Carolina State University.

REFERENCES

Bao, S., S. Raman, and L. Xie, 2003: Numerical simulation of the response of the ocean surface layer to precipitation. *Pure and Applied Geophysics*, **160**, 2419–2446.

Barnes, G., 1994: Summary report of the TOGA COARE international data workshop. Toulouse, France.

Blumberg, A. F., and G. L. Mellor, 1987: A description of a three dimensional coastal ocean circulation model. *Three Dimensional Coastal Ocean Models*, N. Heaps, Ed., American Geophysical Union, 208pp.

Businger, J. A., J. C. Wyngaard, Y. Izumi, and E. F. Bradley, 1971: Flux profile relationship in the atmospheric surface layer. *J. Atmos. Sci.*, **28**, 181–189.

Curry, J. A., and P. J. Webster, 1999: *Thermodynamics of Atmospheres and Oceans*. Academic Press, 254pp.

Emanuel, K., 2001: The contribution of tropical cyclones to the oceans meridional heat transport. *J. Geophys. Res.*, **106**(D14), 14771–14781.

Hong, X. D., S. Raman, R. M. Hodur, and L. Xu, 1999: The mutual response of the tropical squall line and the ocean. *Pure and Applied Geophysics*, **155**, 1–32.

Jorgensen, D. P., T. J. Matejka, and M. A. Le Mone, 1995: Structure and momentum fluxes within a TOGA COARE squall line system observed by airborne Dopplar radar. *21st Conference On Hurricane and Tropical Meteorology, Miami, FL, Amer. Meteor. Soc.*, 579–581.

Kantha, L. H., and C. A. Clayson, 2000: *Numerical Models of Oceansand Oceanic Processes*. Academic Press, 940pp.

Kessler, E., 1969: On the distribution and continuity of water substance in atmospheric circulation. *Meteor. Monogr.*, **32**(10), 84pp.

Levitus, S., and T. P. Boyer, 1994: *World Ocean Atlas 1994. Volume 4: Temperature*. NOAA Atlas NESDIS 4, 129pp.

Levitus, S., R. Burgett, and T. Boyer, 1994: *World Ocean Atlas 1994. Volume 3: Salinity*. NOAA Atlas NESDIS 3, 111pp.

Mellor, G. L., and T. Yamada, 1982: Development of a turbulent closure model for geophysical fluid problems. *Rev. Geophys.*, **20**, 851–875.

Richardson, R. A., I. Ginis, and L. M. Rothstein, 1999: A numerical investigation of the local ocean response to westerly wind burst forcing in the westerly equatorial Pacific. *J. Phys. Oceanogr.*, **29**, 1334–1352.

Trier, S. B., W. C. Skamarock, M. A. Le Mone, and D. B. Parsons, 1996: Structure and evolution of the 22 February 1993 TOGA COARE squall line: Numerical simulations. *J. Atmos. Sci.*, **53**(20), 2861–2886.

Webster, P., and R. Lukas, 1992: Toga coare: The coupled ocean-atmosphere response experiment. *Bull. Amer. Meteor. Soc.*, **73**, 1377–1416.

Wijesekera, H. W., C. A. Paulson, and A. Huyer, 1999: The effect of rainfall on the surface layer in the western equatorial Pacific during a westerly wind burst. *J. Phys. Oceanogr.*, **29**, 612–632.

Xie, L., L. J. Pietrafesa, and S. Raman, 1999: Coastal ocean-atmosphere coupling. *Coastal and Estuarine Studies: Coastal Ocean Prediction*. American Geophysical Union, 101–123.

Xue, M., K. K. Droegemeier, and V. Wong, 2000: The advanced regional prediction system (ARPS)–A multiscale nonhydrostatic atmospheric simulation model, Part I: Model dynamics and verification. *Meteorology and Atmospheric Physics*, **75**, 161–193.